CHAPTER 3

Laser-Based Measurements in Cell Biology

Elliot L. Botvinick[*] and Jagesh V. Shah[†]

[*]Beckman Laser Institute, Department of Biomedical Engineering
University of California, Irvine, California 92612

[†]Laboratory for Cellular Systems Biology and Molecular Imaging, Department of System's Biology
Harvard Medical School, Boston, Massachusetts 02115

In this chapter, we review the imaging techniques and methods of molecular interrogation made possible by integrating laser light sources with microscopy. We discuss the advantages of exciting fluorescence by laser illumination and review commonly used laser-based imaging techniques such as confocal, multiphoton, and total internal reflection microcopy. We also discuss emerging imaging modalities based on intrinsic properties of biological macromolecules such as second harmonic generation imaging and coherent anti-Raman resonance spectroscopy. Super resolution techniques are presented that exceed the theoretical diffraction-limited resolution of a microscope objective. This chapter also focuses on laser-based techniques that can

METHODS IN CELL BIOLOGY, VOL. 82

0091-679X/07 $35.00
DOI: 10.1016/S0091-679X(06)82003-0

report biophysical parameters of fluorescently labeled molecules within living cells. Photobleaching techniques, fluorescence lifetime imaging, and fluorescence correlation methods can measure kinetic rates, molecular diffusion, protein–protein interactions, and concentration of a fluorophore-bound molecule. This chapter provides an introduction to the field of laser-based microscopy enabling readers to determine how best to match their research questions to the current suite of techniques.

I. Introduction

The use of laser sources in microscopy long predate their routine use today in modern cellular-imaging applications such as scanning confocal or multiphoton microscopy (MPM). As outlined in the chapters included in this volume, the first uses of lasers were as sources of high energy light for localized photodamage or microsurgery. Many of the same properties that make them excellent tools for spatially localized damage also provide for high-resolution microscopic imaging and biophysical measurement of molecular parameters within living cells. In part, the wide use of lasers in microscopic imaging, particularly in living cells, has been enabled through the revolution in fluorescent dyes and genetically encoded fluorescent proteins that provide molecular specificity (Shaner *et al.*, 2005; Zhang *et al.*, 2002). In this chapter, we discuss the properties of lasers that make them a unique light source for microscopic imaging and measurement. These properties, such as coherence, monochromaticity, and ultrashort pulses have enabled higher spatial resolution for cellular imaging. More conventional methodologies such as confocal or multiphoton imaging will be discussed alongside some of the recent developments in imaging technologies. Many of the characteristics of lasers also provide the ability to measure molecular parameters within living cells such as protein–protein interactions, diffusion constants, and reaction rates. Many of these measurements have long been considered the domain of *in vitro* systems but now can be interrogated in living cells. The application of lasers to these *in vivo* biophysical methods will also be discussed.

A. The Laser

The laser, originally based on its microwave counterpart the maser of the 1950s, has revolutionized the field of biological measurement. The name laser is an acronym for Light Amplification by Stimulated Emission of Radiation. In a laser, an active laser medium, also referred to as a gain medium, is placed within a resonant optical cavity (for review see Svelto, 1998). An external energy source such as a flash lamp, arc lamp, or light-emitting diode array pumps the electrons of the gain medium into an excited state. If the electrons were allowed to relax to the ground state, spontaneous emission would occur resulting in emitted photons of narrow spectral bandwidth, but of random phase. Instead, a laser uses the principle

of stimulated emission to force the emitted photons into a tightly bound range of phase, frequency, and polarization. Photons traveling back and forth due to reflection from the mirrored walls of the optical cavity bombard the excited atoms of the gain medium. Instead of absorbing the photons, the atoms of the gain media release their potential energy by emitting a second photon similar to the first that travels along the same trajectory. The resonant cavity is designed so that a percentage of light passes through one of the mirrors. The escaped light is the laser beam and is typically collimated, coherent, monochromatic, of constant power, and polarized. This is in stark contrast to light emitted from conventional wide-field illumination sources (e.g., mercury or xenon arc lamps) that are incoherent, of wide spectral content, nonpolarized, and exhibit intensity fluctuations.

B. Coherency and Illumination Volume

Laser light is well suited for fluorescence microscopy because it is spatially and temporally coherent, properties that allow a very tight and bright focus in the specimen plane. Temporal coherency means that the wave is nearly perfectly correlated to itself in time at each point (Svelto, 1998). Spatial coherency means that all points within the wavefront are perfectly cross-correlated, or have similar phase independent of time. Consider, for example, a collimated laser beam incident on the back aperture of a microscope objective lens. The light travels as a coherent plane wave. The microscope objective transforms the plane wave into a converging spherical wave. Because of the coherence of the laser, the resulting focus is nearly diffraction-limited. The laser is ideal in that it minimizes the excitation volume, it provides a "bright" excitation field, and it excites fluorescent molecules with a time-invariant intensity (for the case of continuous wave lasers). Furthermore, using the techniques of Q-switching, mode-locking, or gain-switching, laser output can be transformed from continuous wave to pulsed output. Using pulsed lasers much higher peak irradiances can be achieved in the focal spot. The higher peak irradiances allow for nonlinear interactions, such as multiphoton absorption, between the sample and the light as described in sections below.

II. Laser-Based Imaging Methods

A. Laser Scanning Confocal Microscopy

The most common imaging technology based on laser illumination is confocal microscopy. In 1957, Marvin Minsky proposed a "white light" confocal microscope in which the specimen is scanned by the stage (Inoué, 1995). Later, stage scanning confocal microscopes using laser light sources and nonimaging (photomultiplier tube, PMT) detectors were developed (Wilson, 1980; Wilson *et al.*, 1980) for scanning electronic devices. In the 1980s, laser scanning confocal microscopes (LSCMs) (Carlsson *et al.*, 1985, 1987) came into the forefront in which confocal

fluorescent images of biological specimens were acquired by steering the laser across a stationary specimen. It was apparent that the out-of-focus light rejection and optical-sectioning capability of LSCM over conventional image collection permitted the visualization of individual biological structures never before visualized in fluorescence (White *et al.*, 1987). In conventional laser-based epi-fluorescence, a steep cone of laser light converges to focus, and then diverges out of the specimen. As the cone narrows, irradiance increases with maximum intensity at the focus spot. In order to maximize quantum yield of the fluorescent molecules in the focus spot, illumination power is typically well above the fluorescence threshold (Tsien and Waggoner, 1995). As a result, fluorescence is emitted and subsequently collected by the objective lens from the true focal plane, as well as from out-of-focus objects. In LSCM, laser light is focused into the specimen and excites fluorescence, which passes through a dichroic filter and is reimaged onto the detection pinhole which is placed "confocal" to the laser focus spot (Carlsson and Aslund, 1987; Carlsson *et al.*, 1985). As a result, fluorescence originating from the laser focus passes through the detector pinhole, while that originating from out-of-focus regions does not. Light passing through the pinhole is detected, and by raster scanning the focus spot through the specimen, an image can be constructed. Although the LSCM is rate limited and may adversely effect live cells, it has been used to provide unique insights into neurobiology (Barger *et al.*, 1995; Goodman *et al.*, 1996; Nitatori *et al.*, 1995), HIV (Amara *et al.*, 1997), intracellular signaling (Bae *et al.*, 1997; Hakansson *et al.*, 1998), hepatocyte function (Buchler *et al.*, 1996), intracellular transport (Lin *et al.*, 1995), roles of intracellular calcium (Cheng *et al.*, 1993), carcinogenesis (Aragane *et al.*, 1998), and RNA processing (Spector *et al.*, 1991), just to name a few.

B. Multipoint Confocal Laser Microscopy

One major concern with LSCM is that the high irradiances required to achieve high frame rates and sufficient signal-to-noise ratios adversely effects cell viability. Additionally, because the quantum yield has a finite maximum value, LSCM is inherently rate limited (Gräf *et al.*, 2005). As a solution, multiple confocal pinholes can be implemented and projected into the specimen simultaneously. As the number of pinholes increases, the dwell time per pixel increases proportionally for the same frame rate, and irradiance can be reduced. While attempts have been made to construct and commercialize multipinhole laser microscopes (MPLMs) using technologies such as liquid crystal spatial light modulators (Smith *et al.*, 2000) or micromirror arrays (Fainman *et al.*, 2001; Verveer *et al.*, 1998), the Nipkow spinning disk has become the technology of choice (Conchello and Lichtman, 2005). The Nipkow disk is a spiral array of equally spaced pinholes and was first applied to microscopy by Petrán *et al.* (1968). An expanded laser beam illuminates the disk, while the tube lens together with microscope objective image the illuminated pinholes into the specimen plane. With each rotation of the disk, the entire field is scanned. The Nipkow disk suffers from poor excitation light efficiency, but has nonetheless been successfully commercialized using an arc lamp white light

source (BD Biosciences, California) and has been used in a diverse range of studies including intracellular protein trafficking (Braunagel *et al.*, 2004), nerve myelination (Maria, 2003), and calcium conduction in cerebral endothelia cells (Marrelli *et al.*, 2003). The light efficiency of spinning disk confocal microscopes has been increased to that of LSCM by rotating a second disk containing microlenses coincident with each pinhole of the Nipkow disk. Currently, the CSU10 (confocal scanning unit 10) and the CSU22 from Yokogawa (Yokogawa, Japan) represent the state of the art and scan 20,000 microlenses and pinholes to achieve frame rates of up to 1000 frames per second (Nakano, 2002; Tanaami *et al.*, 2002). For most applications, images are integrated over longer durations and the real benefit of the spinning disk technology over LSCM is cell viability achieved because the necessary irradiance, per pinhole, decreases as the number of pinholes increase for a given frame rate. The Yokogawa spinning disk system is widely used in cell science and has been critical in studies of the cytoskeletal role during cell migration (Adams *et al.*, 2003; Grego *et al.*, 2001; Salmon *et al.*, 2002), the interplay of kinetochores and microtubules during mitosis (Tirnauer *et al.*, 2002), mitotic spindle formation (Ovechkina *et al.*, 2003; Fig. 1), and mitochondrial positioning in yeast (Yaffe *et al.*, 2003).

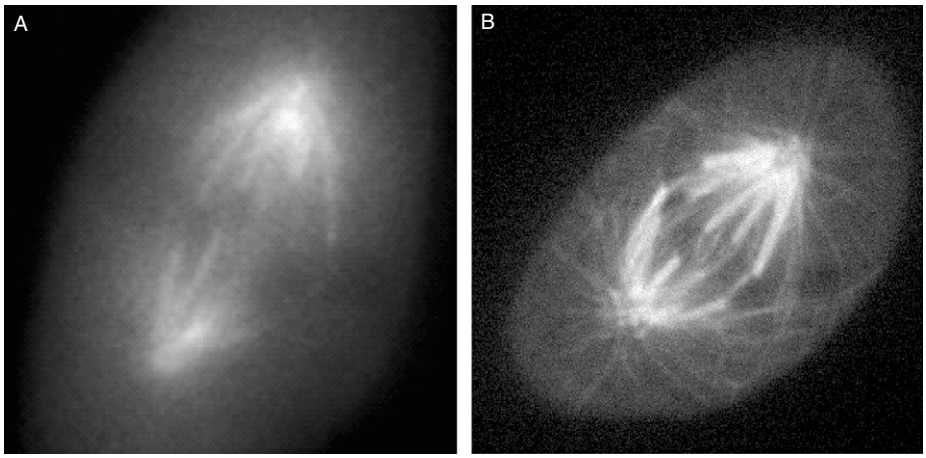

Fig. 1 Confocal microscopy improves spatial resolution within living cells. (A) Conventional epifluorescence image of stable PtK2 cells expressing EYFP-Tubulin. Blurring in the transverse and axial dimensions produces a low resolution and contrast representation of the mitotic spindle. Individual bundles are of poor contrast and single microtubules emanating from the poles are not distinguishable from the background. (B) Image of same cell line acquired by CSU10-based spinning disk confocal head mounted on a Nikon TE2000E2 microscope and illuminated by a mixed gas laser (RM-2018, Spectra-Physics). The improved resolution, particularly in the axial dimension, reveals individual bundles within the mitotic spindle as well as individual microtubules emanating from the spindle poles. Photos courtesy of Jagesh V. Shah and Paul S. Maddox.

C. Total Internal Reflection Microscopy

Total internal reflection microscopy (TIRFM) is a method for imaging cell adhesions, cytoskeletal elements, and membrane components at the glass–cell interface. TIRFM induces total internal reflection between the glass and cell culture media interface sending an evanescent wave a few hundred nanometers deep into the sample with enough irradiance to excite fluorescence. The theory of TIRFM is well described by Reichert and Truskey (1990) and by Gingell *et al.* (1987). The first reported TIRFM system for cells (Axelrod, 1981) implemented a cell culture chamber consisting of a glass coverslip sandwich created by inverting a coverslip containing adhered cells above a second coverslip spaced by a thin membrane. A fused quartz cube was placed on the top coverslip coupled by glycerol. The cube serves to further increase the angle (measured from the optical axis of the objective lens) of laser light from a source sufficiently juxtaposed to the optical axis so that the angle of light between the top coverslip and the cell culture media is greater than the critical angle for total internal reflection. Fluorescence excited by the evanescent wave is collected by the microscope objective and imaged onto a CCD. It is also common to perform TIRFM using only a high numerical aperture objective lens without the relatively complicated setup of the quartz cube-based system (Stout and Axelrod, 1989). Laser light is focused at the back focal plane of the objective, off axis, and at an angle of convergence large enough to illuminate a reasonably large field (Axelrod, 2001a). There are several other schemes for creating TIRFM, reviewed by Axelrod (2001b). Because TIRFM only excites a very thin section of fluorescence at the cell adhesion level, it has enabled several key observations regarding the extent and density of focal adhesions (Mathur *et al.*, 2003), guidance of microtubules to focal adhesions (Krylyshkina *et al.*, 2003), heterogeneity of microtubule-based transport in motile cells (Wadsworth, 1999; Yvon and Wadsworth, 2000), and dynamics of secretory granules (Oheim *et al.*, 1998; Rohrbach, 2000).

D. Nonlinear Imaging

The aforementioned imaging technologies rely on linear absorption of light by molecules to yield fluorescence. In this case, the probability of a fluorescent event is linearly dependent on the beam intensity incident on a fluorescent molecule. A number of imaging modalities are gaining acceptance in cell biology that rely on nonlinear absorption in which the probability of an event (e.g., fluorescence) is not simply proportional to laser intensity (Zipfel *et al.*, 2003). The emergence of nonlinear imaging techniques is in no small part due to the increased availability of turnkey pulsed laser light sources. One such technology is MPM that was first reported by Denk *et al.* (1990). Two-photon absorption was first postulated by Göppert-Meyer (1931) in the 1930s and was first demonstrated shortly after the invention of the laser using a relatively long pulsed laser (ruby laser, $\sim$1 ms pulse duration) to excite a CaF_2:Eu^{2+} crystal (Kaiser and Garrett, 1961). The principle of two-photon absorption is that two photons of near equal energy can interact

with a single molecule as if they were a single photon of twice the energy, if they arrive nearly simultaneously. MPM is an umbrella term that includes not only two-photon absorption, but higher modes of nonlinear absorption as well. In the field of biology, MPM has been demonstrated with continuous wave lasers (Booth and Hell, 1998; Kirsch *et al*., 1998), but in general ultrashort pulse lasers (100 fs or less) in the near infrared (NIR) are used (Curley *et al*., 1992). MPM provides the advantages of confocal optical sectioning, without the need of the detection pinhole. MPM excites with NIR light, which has the advantage over visible light that endogenous absorption by the cells/tissues and water is relatively low compared to the visible spectrum (Konig *et al*., 1995; Liang *et al*., 1996) allowing deeper penetration into tissue samples, multilayer cell cultures, and living tissue. MPM has been used to image pyramidal cells deep within the neocortex (Helmchen and Denk, 2005; Fig. 2), cancerous cell migration in intact tumors (Condeelis and Segall, 2003) and in tissue models (Wang *et al*., 2002; Wolf *et al*., 2003), angiogenesis in the developing brain of zebrafish embryos (Lawson and Weinstein, 2002), dynamic translation rates in living dendrites (Job and Eberwine, 2001), calcium dynamics in living tissues (Denk and Detwiler, 1999; Svoboda *et al*., 1997), and cell fusions in living *Caenorhabditis elegans* embryos (Mohler *et al*., 1998). Single-beam MPM systems suffer the same rate limitations as LSCM. Accordingly, several groups have developed multipoint MPM (MMM) to gain the speed and viability advantages found in spinning disk confocal microscopes (Egner *et al*., 2002). MMM have been developed based on beam splitting (Nielsen *et al*., 2001), a microlens array disk (Bewersdorf *et al*., 1998; Straub and Hell, 1998), and Yokogawa type spinning disk systems (Fujita *et al*., 1999).

Two nonlinear imaging modalities: second harmonic generation (SHG and third THG) and coherent anti-Stokes Raman scattering (CARS) are imaging methods that act on endogenous molecules, rather than through the introduction of fluorescent reporters. SHG microscopy, based on a 1978 publication first suggesting the imaging modality (Sheppard and Kompfner, 1978), was first applied to biological tissue by Freund and Deutsch (Freund and Deutsch, 1986; Freund *et al*., 1986) who examined collagen structure in the rat tail tendon. SHG, or frequency doubling, is a nonlinear process requiring high irradiance illumination through a highly polarizable material with a noncentrosymmetric molecular organization (Campagnola and Loew, 2003). SHG emits light at half the wavelength of the excitation illumination so that two NIR photons from a femtosecond pulsed laser typically used in two-photon microscopy would create a single photon in the visible spectrum at twice the energy. Since SHG is dependent on the scale and the form of molecular ordering within the tissue (Freund and Deutsch, 1986; Zipfel *et al*., 2003) and collagen is highly organized in the tendon, the method yields high contrast signals in that tissue. SHG has been shown to produce optically sectioned images of the plasma membrane (Campagnola *et al*., 2002; Peleg *et al*., 1999), tumor development in hamster cheek pouch mucosa (Guo *et al*., 1999), collagen in RAFT tissue models (Zoumi *et al*., 2002), and sarcomeres with the *C. elegans* nematode (Campagnola and Loew, 2003; Fig. 3). CARS is a type of multiphoton "vibrational imaging"

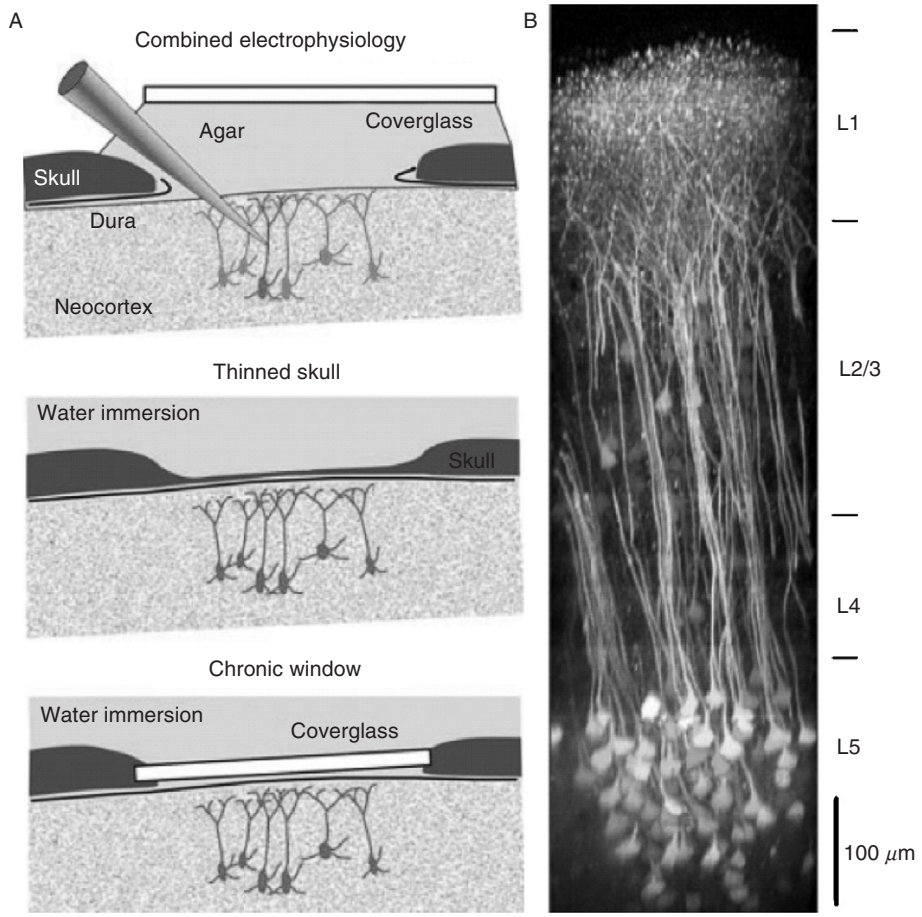

Fig. 2 *In vivo* two-photon imaging in the intact neocortex. (A) Different types of brain access. Open cranial window with the dura mater removed so that micropipettes for cell labeling and electrophysiological recordings can be inserted (top). Pulsation of the exposed brain is reduced by covering the craniotomy with agar and a coverglass. Thinned skull (20- to 4-μm thickness) preparation (middle). Cellular structures are either prelabeled (e.g., with fluorescent proteins in transgenic mice) or stained through a tiny hole lateral to the thinned area. Chronically implanted glass window replacing the skull (bottom). Agar is used underneath the window for stabilization. (B) Example of deep two-photon imaging in mouse neocortex. Maximum intensity side projection of a fluorescence image stack, obtained in a transgenic mouse expressing Clomeleon, a genetically encoded chloride indicator, under the control of the Thy1-promoter, preferentially in deep layer 5 (L5) pyramidal cells. Data were taken with a 10-W pumped Ti:Sapphire oscillator using a 40, NA 0.8 water immersion lens (Zeiss). Note that nearly the entire depth of the neocortex can be imaged. Reprinted by permission from Macmillan Publishers Ltd., Nature (Helmchen and Denk, 2005), copyright (2006).

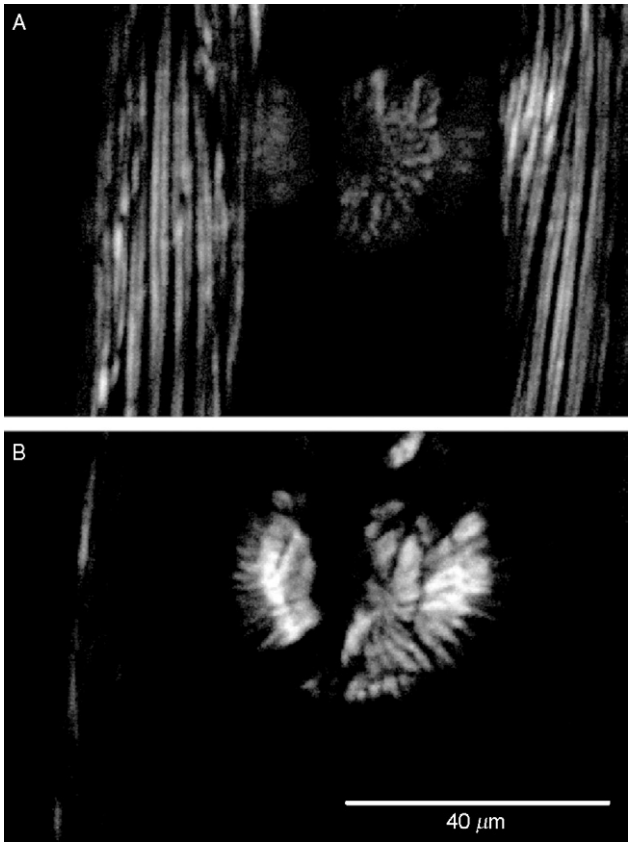

Fig. 3 SHG provides optical sectioning from endogenous molecules. Endogenous SHG imaging of a living adult *C. elegans* nematode, showing two distinct axial slices. (A) The sarcomeres in the body wall muscles are seen at the edges of the animal, as well as in a portion of the chewing mechanism. (B) An optical section further into the same animal, where only the chewing mechanism is observed with substantial SHG intensity. Reprinted by permission from Macmillan Publishers Ltd., Nature (Campagnola and Loew, 2003), copyright (2003).

based on coherent anti-Stokes Raman scattering in which three electric fields: the pump, Stokes, and probe interact with molecules in a sample to generate the anti-Stokes signal (Cheng and Xie, 2004; Duncan *et al.*, 1982; Tolles *et al.*, 1977). Molecular specificity is achieved from characteristic molecular vibrations of endogenous species. CARS is still an experimental technology and has not yet moved into mainstream imaging. It has been used to image lipids in live cells (Chen *et al.*, 2002), to determine the thermodynamic state (liquid crystalline or gel phase) of lipid membranes (Muller and Schins, 2002), to image neutral lipid droplets (LDs) in unstained live fibroblasts (Nan *et al.*, 2003), and to measure real-time intracellular water concentrations in live cells (Potma *et al.*, 2001). CARS has been used to image

intact tissues including lipid domains in the mouse ear *in vivo* (Evans *et al.*, 2005), and lipid phase within axonal myelin in live spinal tissue explants (Wang *et al.*, 2005).

E. Super Resolution Microscopy

Lasers can be used to stretch the resolution of microscopy beyond the diffraction limit of light. For example, TIRFM improves axial resolution beyond the diffraction limit because the evanescent field extent is smaller than the axial extent of the point spread function (PSF) of a focused laser. Using acoustic optical modulators to vary the angle of laser incidence in TIRFM with subsequent Laplace transform-based reconstruction, topographical resolutions of tens of nanometers have been achieved (Loerke *et al.*, 2000).

In standing wave fluorescence microscopy two coherent plane waves, either from two apposing objective lenses, or from a single objective opposing a piezo-controlled mirror, interfere in the specimen plane to yield an axial resolution better than 0.05 μm (Bailey *et al.*, 1993). The 4Pi confocal fluorescence microscope presented by Hell and Stelzer (1992b) uses two apposing 1.4 NA objectives to optically compensate for axial spreading of the PSF to achieve 110 nm axial resolution (vs the diffraction limit of $\sim$1 μm) in Nile Blue dye. In type A 4Pi confocal microscopy, both objectives focus a laser beam to a common focal point where constructive interference occurs and the resulting illumination PSF takes on a more spherical geometry thereby reducing axial stretching. In type C 4Pi confocal microscopy, resolution is further enhanced by interference of detected light on a common point detector. The 4Pi design has also been shown to improve two-photon microscopy (Hell and Stelzer, 1992a).

III. Measurement of Cellular State: Molecular Parameters

A central feature in fluorescent imaging is the ability to determine the position and relative levels of a specific molecule. Lasers, as described above, act to provide better spatial resolution and multiplexed detection than conventional light sources due to their coherence and monochromaticity. The ability to provide a high flux of photons to a small diffraction-limited volume can also be used to modulate fluorescent molecules at a specific location or measure the properties of fluorescent molecules. Below we survey a number of biophysical measurements techniques used in living cells that have been enabled or improved by the use of lasers.

A. Photobleaching Methods

1. General Principle

In this family of methods, a protein (or other cellular component) is labeled with a fluorophore and permitted to equilibrate in the cell. Through the use of a laser, a region of these fluorescent molecules can be excited sufficiently so that they

are no longer fluorescent, that is undergo photobleaching. These bleached molecules now represent a new species that can be distinguished from the existing fluorescent pool. The kinetics of these molecules can provide a quantitative insight into various physical processes such as diffusion, reaction, and flow. The experimental measurement described above is often referred to as fluorescence recovery (or redistribution) after photobleaching (FRAP).

2. Microscopy Configurations

Practical photobleaching is accomplished via high-intensity light source, such as a laser, that excites the fluorophore with a sufficient number of photons to make the probability of losing its fluorescence significantly large. Many LSCMs can be used as FRAP setups, by increasing the laser intensity in a small region for photobleaching and then lowering the power for imaging the subsequent recovery dynamics. Other setups also use a laser to achieve a diffraction-limited spot of high illumination that is used for single-point FRAP and imaging is then usually achieved by another light source such as an arc lamp. Scanning confocals can photobleach regions of arbitrary shape and size, via the use of the scanhead, permitting the bleaching of a subregion of a fluorescently labeled organelle such as the nucleus (Daigle *et al.*, 2001). Single-point FRAP configurations can accomplish spatial-patterning FRAP through the use of galvanometers that move the laser or lenses that can change the focused beam into lines or more complex shapes.

Some experimental setups utilize lower intensity sources (e.g., mercury or xenon arc lamps) and arise to bleach molecules but require an extended time period to achieve a detectable bleached pool. These longer exposure times compete with intrinsic diffusive mechanisms that permit mixing of the ''bright'' and ''dark'' species during the photobleaching period and thus the FRAP dynamics become a complex mix of photobleaching and recovery kinetics. To measure dynamic processes with fast timescales (on the order of tens of seconds to many minutes), a laser is essential to provide a high-intensity flux of photons that can rapidly bleach, and therefore mark, the fluorescent molecules of interest.

3. Measurement Data and Interpretation

In a typical FRAP experiment, the recovery at the point of photobleaching is monitored. This measurement is often made via quantitative imaging but can also be carried out using low-intensity laser excitation to measure local fluorescence. The basic FRAP recovery curve consists of the initial fluorescence level, the bleaching event which reduces the amount of fluorescence and the recovery to a new steady state (Fig. 4). The key parameters in the recovery curve are the rate and extent of recovery. These parameters are obtained by fitting the recovery curve to an exponential recovery equation [Eq. (1)]

$$\bar{F}(t) = A(1 - e^{-1/\tau}) \tag{1}$$

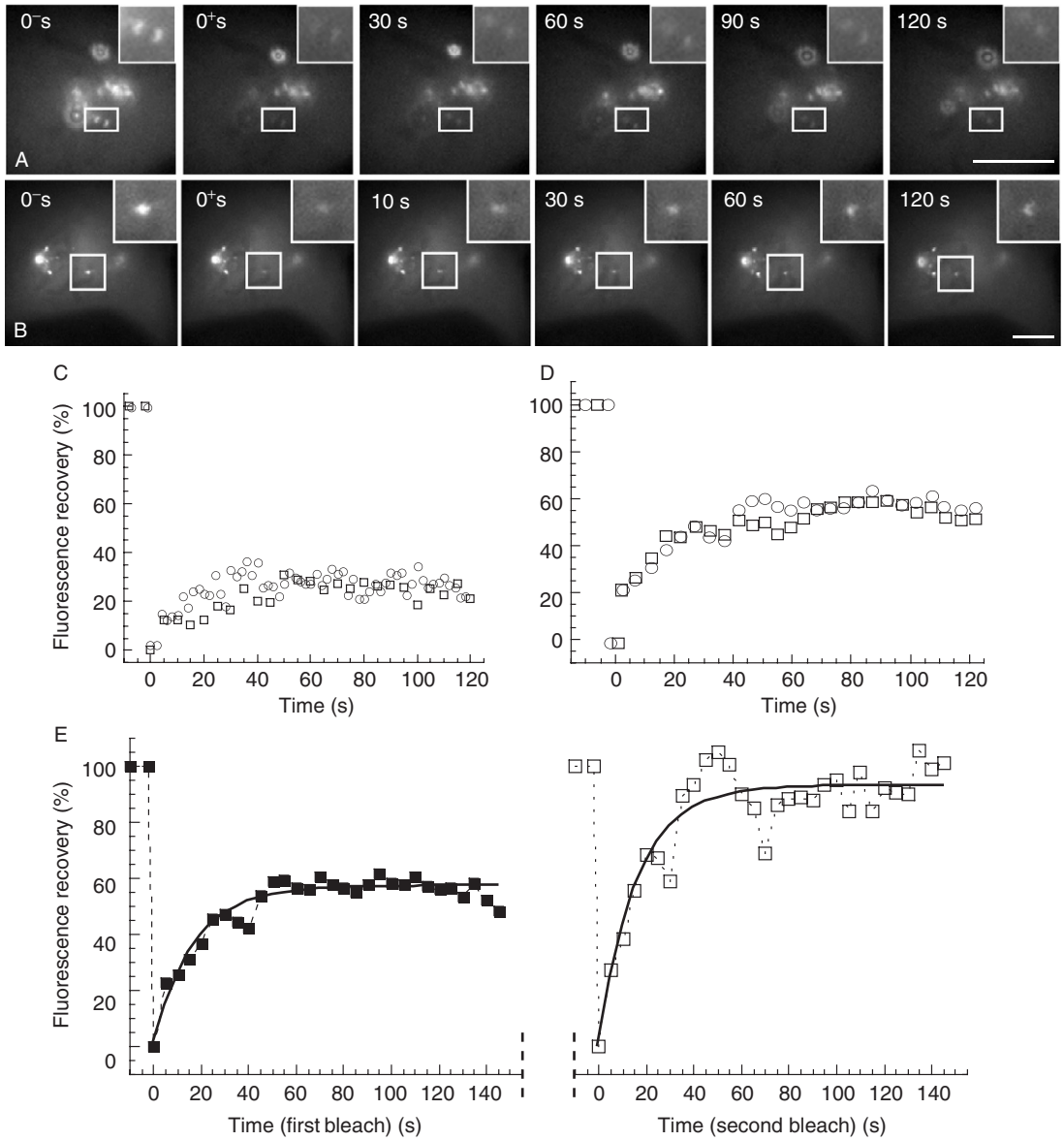

Fig. 4 Fluorescence recovery after photobleaching measurements in living cells. Photobleaching of a mitotic kinetochore protein Mad1 (A) and Mad2 (B) each fused to yellow fluorescent protein (EYFP) stably expressed in PtK2 cells was accomplished with the 532-nm line of an Nd:YAG laser. Quantification of fluorescence recovery at mitotic kinetochores for both Mad1 (C) and Mad2 (D and E) demonstrates that Mad1 recovers to ~25% its original fluorescence over the 5-min time period. However, Mad2 recovers to a level of ~50% (D) which upon serial photobleaching of the same kinetochore recovers to 100% of the prebleach value (E). These data reveal a relatively stable pool of Mad1 but a complex mixture of a stable and transient pool of Mad2 at the unattached kinetochore. Reprinted by permission from Elsevier (Shah *et al.*, 2004), copyright (2004).

where $\bar{F}(t)$ represents the normalized fluorescence of the region that incorporates the initial region fluorescence, fluctuations of the light source, and bleaching due to observation. Recovery curves often exhibit single exponential recovery kinetics with a single recovery time (τ) and extent (A). In more complex kinetics, recovery curve fitting requires modeling the existence of multiple components of recovery [Eq. (2)]

$$\bar{F}(t) = \sum_i A_i(1 - e^{-1/\tau_i}) \tag{2}$$

where each component is parameterized by its time of recovery (the exponential decay term, τ_i) and contribution to extent of recovery (A_i). The extent of recovery is a direct readout of the mobility of the fluorescent moiety in the region. A high extent of recovery indicates a transient interaction at some subcellular scaffold or complete diffusive recovery in a membrane or cytoplasmic compartment. Low extent of recovery indicates a significant immobile fraction ($1 - A$ or $\sum_i A$) that may turnover on timescales longer than that of the experimental measurement (Fig. 4). The time of recovery indicates the timescale of diffusion, reaction kinetics or flow, whichever is the dominant process at work. The interpretation of the recovery time depends greatly on the underlying biology under study. Two simple model systems are the *in vitro* fluid membrane (or *in vitro* solution) and the insoluble scaffold. Within simple *in vitro* soluble systems, a single exponential recovery rate can be readily converted into a diffusion constant, whereas at insoluble scaffolds, the recovery rate is directly related to the off-rate ($1/\tau$) of the reaction between the fluorescent marker and the scaffold (Axelrod *et al.*, 1976; Braeckmans *et al.*, 2003; Bulinski *et al.*, 2001; Lele and Ingber, 2006; Sprague *et al.*, 2004). These two extremes represent the simplest systems in which we can find direct interpretation of the recovery time. *In vivo* cellular measurements can be complicated by the complex structure of membranes and the cytoplasm. However, in combination with a model of the underlying biology, FRAP experiments can reveal kinetic phenomena otherwise inaccessible via fluorescence imaging alone and provide a quantitative measurement of these kinetics.

4. Cellular Applications

Early work using FRAP measured the diffusion of fluorescent reporters within the plasma membrane and laid the groundwork for studies of kinetics and diffusion in many other systems (Axelrod *et al.*, 1976; Jacobson *et al.*, 1976). Since that time, FRAP has been widely employed within many areas of cell biology. Work by Luby-Phelps and Taylor (1988) provided the first measurements of the heterogeneity of diffusion in the cellular cytoplasm using fluorescently labeled dextrans introduce by microinjection. Membranous organelles, such as the nuclear envelope (Daigle *et al.*, 2001), have been studied extensively to dissect the ability of proteins to freely diffuse within the membrane (Axelrod *et al.*, 1976; Jacobson *et al.*, 1976) or membranous compartments (Nehls *et al.*, 2000).

FRAP has also found tremendous utility in the study of nuclear and chromosome dynamics, in part due to the stable nature of some protein scaffolds found near or on chromatin such as chromosomes and kinetochores (Gerlich *et al*., 2006; Howell *et al*., 2000; Shah *et al*., 2004), DNA damage machinery (Bekker-Jensen *et al*., 2005) and nucleoli (Chen and Huang, 2001), and other more transiently bound nuclear components (Misteli *et al*., 2000). Similarly, studies related to the cytoskeleton (Bulinski *et al*., 2001; Pearson *et al*., 2003) and cytoskeletal-associated structures (Khodjakov and Rieder, 1999; Kisurina-Evgenieva *et al*., 2004; von Wichert *et al*., 2003) use FRAP as a central methodology to investigate dynamics of protein association and turnover.

5. Related Methodologies

Modified experimental setups can also monitor the loss in fluorescence that occurs far from a position undergoing constant photobleaching (Delon *et al*., 2006; Wachsmuth *et al*., 2003). Through constant photobleaching of fluorescent molecules in one compartment and simultaneously monitoring the loss in fluorescence in another, the dynamic exchange between the compartments can be established. These fluorescence loss in photobleaching or FLIP experiments can provide insight into diffusion and transport that occur between different cellular compartments, for example cytoplasm and nucleus (Belaya *et al*., 2006; Shimi *et al*., 2004) or nuclear and subnuclear compartments (Chen and Huang, 2001).

Following the trajectory of bleached molecules by FRAP can also be accomplished by the use of photoactivation of fluorescence or photoconversion. FLAP or fluorescence localization after photoactivation (or photoconversion) follows the emergence of a new fluorescent species that is produced through the action of a laser or high-intensity light source. Fluorescence activation was originally performed by a high-intensity ultraviolet source that ''uncaged'' or cleaved a chemical moiety that prevented fluorescence (Mitchison, 1989). Such methods found widespread utilization in dynamical cell processes such as cell division (Mitchison, 1989) and cell motility (Theriot and Mitchison, 1991), although the ''caged'' fluorophores had to be introduced through cellular microinjection. The development of a photoactivatable green fluorescent protein mutant (PA-GFP) (Patterson and Lippincott-Schwartz, 2002) and the photoswitchable fluorescent protein Dronpa (Habuchi *et al*., 2005) have enabled genetic tagging of proteins and their subsequent activation within living cells without microinjection. Such proteins have been used in dynamic cellular processes such as cell division (Salic *et al*., 2004). In addition to the activation of fluorescence, a number of proteins have been developed that dramatically change their fluorescent spectra on exposure to ultraviolet wavelengths. Kaede (Ando *et al*., 2002), EosFP (Wiedenmann *et al*., 2004), and KikGR (Tsutsui *et al*., 2005) exhibit dramatic red-shifted spectral shifts in emission providing a spectrally distinct fluorophore after photoconversion. A simple photoconvertible fluorescent protein tag has also been developed by utilizing the efficient energy transfer between concatenated cyan and yellow fluorescent proteins. Without perturbation, excitation of the cyan fluorescent

protein produces yellow emission, but after bleaching of the yellow fluorescent protein undergoes a dramatic donor-dequenching producing primarily cyan emission (Shimozono *et al.*, 2006). These proteins represent the state-of-the-art in fluorescence dynamics reporters and should enjoy great success in cell biological applications where dynamic measurements are required.

B. Fluorescence Lifetime Imaging

1. General Principles

While FRAP-based techniques developed from imaging-based modalities, fluorescence spectroscopy techniques have proved to be a driving force for the innovation in microscopy-based biophysical measurements in living cells (Lakowicz, 1999). One such example is fluorescence lifetime imaging (FLIM). The lifetime of a fluorophore is a result of stochastic nature of spontaneous emission of photons from a population of excited fluorophores. The excited fluorophores, when excited nearly simultaneously, do not synchronously emit singlet transition photons, but instead have a characteristic average timescale of transition. Rapid time-resolved measurements after short-pulsed excitation of an ideal fluorophore reveal a single exponential decay in emission intensity. This decay constant is the lifetime of the fluorophore. The lifetime of a fluorophore can be exquisitely sensitive to its surroundings providing a unique measure of local state. Moreover, the measurements of anisotropy (another form of lifetime measurement) as a result of polarized excitation and emission can provide quantitative measurements of rotational diffusion. FLIM techniques are still actively being developed as is the analysis, but its utility in the realm of energy transfer [Fluorescent (or Förster) resonant energy transfer, FRET] measurements, has already provided significant momentum in its use in cell biology.

2. Microscopy Configurations

As with cuvette-based fluorescence spectroscopy measurements, laser-based microscopy provides two methods for the measurement of fluorescence lifetimes. Frequency-domain measurements drive fluorophores with a signal rapidly modulated intensity and detect the modulated response at the detector. Driving the fluorophores with a modulated intensity with varying periods near the fluorescence lifetime results in an emission signal shifted in phase and modulated in amplitude due to the lifetime decay (Harpur *et al.*, 2001). Frequency-domain methods can be implemented on LSCMs, but equivalently can also be done in wide-field microscopy by illuminating the entire microscope field with a modulated excitation. The ability to image by wide-field provides a rapid method of measuring lifetimes on a pixel-by-pixel basis, at a cost of requiring expensive cameras for sensitive detection. The frequency-domain methods, however, can require complex excitation protocols and calculations in the presence of multiple lifetimes (Bastiaens and Squire, 1999).

To accurately resolve multiple lifetimes, time-domain measurements use a pulsed laser to rapidly excite the fluorophores in a small region of the microscope field

and detect the emission profile in time. The time-resolved measurements of the fluorescence decay can be evaluated at each scanned position of the laser and the fluorescence lifetime image is thus built pixel-by-pixel. Such time-resolved measurements can also be made on an LSCM equipped with high-time resolution detectors. Here the confocal laser source would not be a continuous wave laser, but a pulsed source of femtosecond to picosecond duration. Many multiphoton scanning microscopes already have much of the hardware for fluorescence lifetime imaging through the use of the pulsed infrared source and nonimaging detectors (Becker *et al.*, 2004).

3. Measurement Data and Interpretation

Frequency-domain measurements use the change in amplitude and phase that occurs as the input signal passes through the fluorescent samples. The calculations result in two lifetimes, one based on the change in amplitude and one based on the change in phase (outlined in French *et al.*, 1998; Lakowicz, 1999). For modulation input periods close to the single fluorescence lifetime in the sample, these values will be similar, but when multiple species are present or if single fluorescent species have multiple lifetimes, these values differ and computation of the lifetimes requires more involved calculations (Harpur *et al.*, 2001). Time-resolved measurements involve fitting the exponential decay captured after the pulsed excitation of the sample. This decay can be directly fit with single or multiple exponentials to obtain the fluorescence lifetimes present in the sample (Lakowicz, 1999).

4. Cellular Applications

Lifetime measurements have enjoyed great success in the area of energy transfer measurements in living cells. FRET is a phenomenon by which excitation of a donor fluorophore results in the emission of acceptor fluorophore through a nonradiative mechanism. The length scale for this transfer must be in the range of 2–7 nm and decays with the sixth power of the increasing distance (Bastiaens and Squire, 1999). This strong distance dependence provides exquisite sensitivity for detecting protein–protein (or other molecular) interactions within living systems. Intensity-based measurements of FRET can be problematic due to the relative concentrations of acceptor and donor fluorophores as well as cross-talk between fluorescent spectra (Jares-Erijman and Jovin, 2003), particularly when using fluorescent protein fusions (Pelet *et al.*, 2006). One interesting result of energy transfer is the reduction in fluorescence lifetime of the donor fluorophore when undergoing energy transfer. Using a variety of measurement modalities, FRET detection via fluorescence lifetimes have become increasingly popular in cell biology applications (Caudron *et al.*, 2005; Delbarre *et al.*, 2006; Kalab *et al.*, 2006; Peter *et al.*, 2005; Ramdya *et al.*, 2003; Fig. 5). Moreover, the possibility of multiphoton excitation provides for measurements made deep within tissues to detect protein–protein interactions within living organisms (Chen and Periasamy, 2004).

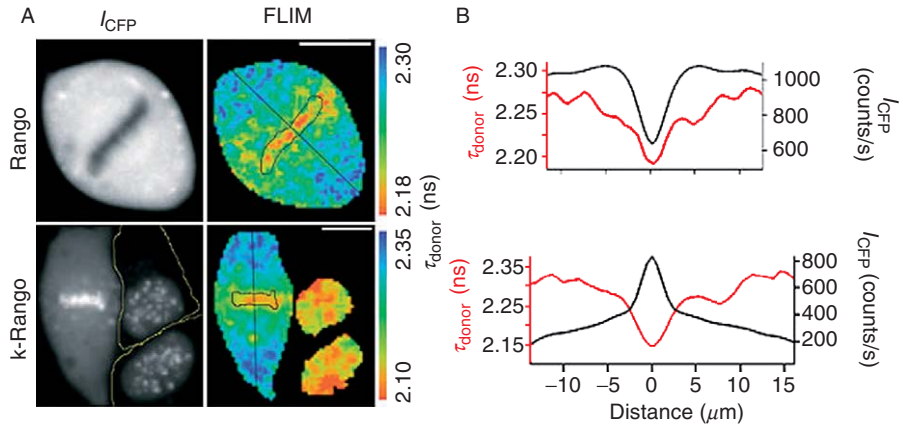

Fig. 5 Fluorescence lifetime/energy transfer imaging within living cells. (A) An FRET probe composed of an ECFP–EYFP fusion (Rango) separated by an Importin-β (protein)-binding domain reports on unbound probe near chromosomes in mitotic cells. The measurement of a control fusion protein (k-Rango) demonstrates a distinct localization but similar lifetime image indicating the specificity of the probe for reporting Importin-β binding. (B) Linescan measurements of fluorescence lifetime and donor fluorescence display similar lifetime profiles bur distinct donor intensities demonstrating the difference between the simple image intensity and the energy transfer reporting an underlying biochemical interaction. Reprinted by permission from Macmillan Publishers Ltd., Nature (Kalab *et al.*, 2006), copyright (2006).

Lifetime imaging has also been applied to measurements of protein mobility through the use of polarization/anisotropy methods (Clayton *et al.*, 2002; Dix and Verkman, 1990). These techniques provide measures of rotational mobility and are very sensitive to changes in protein size. Rotational correlation times of proteins are generally in the area of tens of nanoseconds. Unfortunately, GFP mutants with lifetimes in the range of ~1–3 ns (Tsien, 1998; Volkmer *et al.*, 2000) cannot provide the temporal resolution for such measurements. As a result, live cell anisotropy measurements for molecular mobility studies require nongenetically encoded fluorophores with long fluorescent lifetimes that need to be covalently coupled to the molecule of interest and directly introduced into the cellular environment. It should be noted, however, that GFP mutants do exhibit significant differences in fluorescence lifetimes, a property that can be exploited for imaging fluorescent proteins with large spectral overlap in emission (Harpur *et al.*, 2001).

C. Fluorescence Correlation Spectroscopy

1. General Principles

Fluorescence correlation spectroscopy (FCS) has become an increasingly popular tool in cell biology due to its ability to discern changes in biological complex size, concentration, and composition in living cells (Medina and Schwille, 2002).

FCS techniques use a laser to produce a small excitation volume (~0.1 to tens of femtoliters) from which the fluctuations in fluorescence are measured at high time resolution (approximately tens of nanoseconds). The origin of the fluctuations can be a result of photophysical processes, reaction kinetics, diffusion, and flow (Magde *et al.*, 1972). Photophysical processes and reaction kinetics have timescales shorter than the average residence time of the fluorophore within the excitation volume, whereas fluctuations due to diffusion and flow are a result of fluorescent molecules leaving and entering the excitation volume. The time average of these fluctuations can also provide the absolute concentrations of fluorescent molecules. The ability to measure such a wide variety of biophysical processes and make absolute measurements of concentration has fueled interest in the use of FCS-based techniques in cell biology.

2. Microscopy Configurations

FCS measurements can be made using a variety of microscope configurations. Basic requirements are a laser to produce the small excitation volume, a high-sensitivity or high time resolution detector [e.g., avalanche photodiode (APD) or PMT], and hardware to convert the measured detection signal into a digital form (Schwille *et al.*, 1999).

Confocal excitation with a continuous wave laser requires a pinhole at the detector to exclude out-of-focus excitation, similar to those already present in laser scanning confocals. Multiphoton excitation does not require the pinhole since only the volume of interest is excited making detection hardware simpler, at the expense of more complex and expensive ultrafast lasers (e.g., Ti:Sapphire femtosecond sources) (Berland *et al.*, 1995; Wang *et al.*, 2006).

Detection hardware can vary depending on the application. High-sensitivity applications, such as measuring low concentrations of fluorescent molecules (~10 pM), require the use of APDs, whereas less sensitive applications can use PMTs. High-time resolution are features of both detectors; however, many single-color FCS configurations use two detectors at half the intensity and cross-correlation, to reduce noise and after-pulsing that may be present in the detectors. This can greatly increase the effective time resolution of the instrument.

Correlation measurements to determine molecular photophysics or mobility can be accomplished online through fast hardware autocorrelators. Alternatively, photon-counting cards with high bandwidth can be used to record fluctuation time series directly and correlation can be done offline. Direct fluctuation recordings can be used in related fluctuation spectroscopy methods such as photon-counting histogram analysis (Chen *et al.*, 1999).

3. Measurement Data and Interpretation

A central feature of FCS measurements is the underlying model of fluorescence fluctuations. Within living cells dynamics of reaction kinetics are relatively slow, particularly when compared to average residence times within the subfemtoliter

excitation volume. As a result, most fluctuations are due to the entry and exit of fluorescent species permitting the measurement of a diffusion constant (or equivalently the size of a complex) and concentration. The diffusion constant of the complex of interest can be determined both in the 3D space of the cytoplasm or 2D plane of the membrane. In both cases, the diffusion constant can be derived from fits to the autocorrelation function of the fluorescence fluctuations (Schwille *et al*., 1999). The equations to fit the autocorrelation decay curve, a measure of the residence time of the fluorescent molecules also contain the average number of molecules contained within the volume. Thus, the fits to the decay curve, even for a single fluorescent species, require two free parameters (Fig. 6). Another parameter derived from the microscope configuration is the excitation volume. This volume can be calibrated by using molecules with a known diffusion constant and at known concentrations and is a sensitive parameter in the fitting of the autocorrelation function. The ability to evaluate absolute concentrations within the cellular environment can be challenging, but relative concentrations can be evaluated with high confidence to follow the dynamic changes in complex formation and dissociation

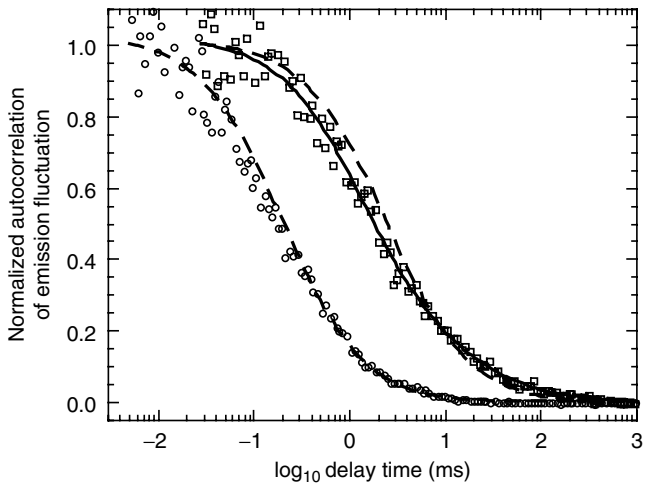

Fig. 6 Fluorescence correlation spectroscopy *in vitro* and within living cells. Fluorescence emission autocorrelation function resulting from Multiphoton excitation of recombinantly expressed cyan fluorescent protein (ECFP) fused to the mitotic checkpoint protein Mad2 (left curve and points) and within PtK2 cells stably expressing ECFP fused to Mad2 (right curves and points). Excitation was accomplished with the 800-nm line of a Ti:Sapphire femtosecond pulsed laser. The *in vitro* measurements demonstrate the fast residence times of *in vitro* proteins (diffusion constant of ~80 $\mu m^2/s$) versus the intracellular measurements resulting in a effective increase of about cytoplasmic viscosity by a factor of four (small complex ~21 $\mu m^2/s$, large complex ~1 $\mu m^2/s$, relative concentration ratio of 6:1, small to large). The intracellular measurements indicate that the Mad2 protein exists in two major complexes in mitotic cells (one component fit — — dashed line, two component fit — solid line) seen by the poor one component fit at long residence times. Only the small complex is present in nonmitotic cells, indicating a mitosis-specific assembly process.

(Wang *et al.*, 2006). In addition, a number of elements such as excitation power, shape of the excitation volume as well as the geometry and obstacles within the cell must all be considered in evaluating the parameters that result from the fit of the autocorrelation function (Berland *et al.*, 2003; Hess *et al.*, 2002; Nagy *et al.*, 2005). With these factors taken into account carefully, FCS can be a unique tool for measurements of cellular biochemistry.

4. Cellular Applications

FCS measurements in living cells are becoming increasingly popular, particularly with the introduction of commercial systems available as additions to scanning confocal microscopes. There has been a great deal of detailed measurement of GFP and its variants to understand the nature of the fluorophore both *in vitro* (Chen *et al.*, 2002) in the cellular environment (Schwille *et al.*, 1999; Wang *et al.*, 2004; Fig. 6). Measurements of intracellular protein dynamics have made important insights into retroviral assembly (Larson *et al.*, 2003), intracellular motility (Kohler *et al.*, 2000), cytoplasmic structure (Weiss *et al.*, 2003), and cell cycle control (Wang *et al.*, 2006). On-going developments in fluorescent proteins and fluorophores (Kogure *et al.*, 2006) and data analysis methods (Chen *et al.*, 1999, 2005; Muller, 2004) promise to provide new insights into cellular dynamics.

5. Related Methodologies

FCS methodologies are being actively developed and the list of related methodologies is changing rapidly (Breusegem *et al.*, 2006). One technique that is particularly well suited to cellular studies is fluorescence cross-correlation spectroscopy (FCCS). Here two spectrally distinct fluorescent species are monitored in the cytoplasm or within the cellular membrane. Autocorrelation analysis of each color separately provides the concentration and diffusion constant parameters previously described. However, cross-correlation between the channels provides concentration and diffusion parameters on complexes containing both fluorophores. Much like FRET, the result is the ability to monitor protein–protein interactions but without the requirement for close apposition of the fluorophores. FCCS-based protein–protein interactions are detected on the basis of the correlated motions into and out of the excitation volume (Bacia *et al.*, 2006). FCCS measurements provide the composition of the complexes, an element not available through single color FCS. Recent work has used FCCS to monitor receptor–ligand interactions (Larson *et al.*, 2005), calcium-signaling (Kim *et al.*, 2005), and *in vivo* protease activity (Kogure *et al.*, 2006).

Many FCS/FCCS instruments are configured for single-point measurements making spatial diffusion maps and spatial cross-correlation measurements impossible. Developments have incorporated position information into FCS measurements providing spatial and temporal correlation profiles (Digman *et al.*, 2005; Sisan *et al.*, 2006; Skinner *et al.*, 2005; Ries and Schwille, 2006). Cross-correlation

in time and space will provide novel methods of analyzing cellular complex dynamics and reaction kinetics all within the living cell.

New developments in FCS and FCCS through novel fluorescent proteins that permit single color excitation dual-color emission FCCS or optical configurations for interleaved dual-color excitation (Thews *et al.*, 2005) as well as position scanning are moving the field toward simpler instruments to extract molecular dynamics and protein–protein interactions as they occur in living cells.

IV. Summary

We have presented an overview of the leading and emerging technologies in laser-based imaging and molecular state measurement. While several of these techniques had been proposed in the years preceding laser development, the widespread commercialization and distribution of continuous wave and pulsed laser systems has brought molecular characterization into the biology research laboratory. The transformation of laser systems from the intimidating research platform architecture into the ''friendly,'' closed system ''turnkey'' architecture is a clear indication that lasers are becoming ubiquitous tools in the biological laboratory. The availability of these turnkey laser systems has enabled the cell biologist to bring a host of techniques that permit imaging and molecular measurements to the study of the biochemical basis of cellular function.

References

Adams, M. C., Salmon, W. C., Gupton, S. L., Cohan, C. S., Wittmann, T., Prigozhina, N., and Waterman-Storer, C. M. (2003). A high-speed multispectral spinning-disk confocal microscope system for fluorescent speckle microscopy of living cells. *Methods* **29**(1), 29–41.

Amara, A., Legall, S., Schwartz, O., Salamero, J., Montes, M., Loetscher, P., Baggiolini, M., Virelizier, J. L., and Arenzanaseisdedos, F. (1997). HIV coreceptor downregulation as antiviral principle: SDF-1 alpha-dependent internalization of the chemokine receptor CXCR4 contributes to inhibition of HIV replication. *J. Exp. Med.* **186**(1), 139–146.

Ando, R., Hama, H., Yamamoto-Hino, M., Mizuno, H., and Miyawaki, A. (2002). An optical marker based on the UV-induced green-to-red photoconversion of a fluorescent protein. *Proc. Natl. Acad. Sci. USA* **99**(20), 12651–12656.

Aragane, Y., Kulms, D., Metze, D., Wilkes, G., Poppelmann, B., Luger, T. A., and Schwarz, T. (1998). Ultraviolet light induces apoptosis via direct activation of CD95 (Fas/APO-1) independently of its ligand CD95L. *J. Cell Biol.* **140**(1), 171–182.

Axelrod, D. (1981). Cell-substrate contacts illuminated by total internal reflection flourescence. *J. Cell. Biol.* **89,** 141–145.

Axelrod, D. (2001a). Selective imaging of surface fluorescence with very high aperture microscope objectives. *J. Biomed. Opt.* **6**(1), 6–13.

Axelrod, D. (2001b). Total internal reflection fluorescence microscopy in cell biology. *Traffic* **2**(11), 764–774.

Axelrod, D., Koppel, D. E., Schlessinger, J., Elson, E., and Webb, W. W. (1976). Mobility measurement by analysis of fluorescence photobleaching recovery kinetics. *Biophys. J.* **16**(9), 1055–1069.

Bacia, K., Kim, S. A., and Schwille, P. (2006). Fluorescence cross-correlation spectroscopy in living cells. *Nat. Methods* **3**(2), 83–89.

Bae, Y. S., Kang, S. W., Seo, M. S., Baines, I. C., Tekle, E., Chock, P. B., and Rhee, S. G. (1997). Epidermal growth factor (EGF)-induced generation of hydrogen peroxide—role in EGF receptor-mediated tyrosine phosphorylation. *J. Biol. Chem.* **272**(1), 217–221.

Bailey, B., Farkas, D. L., Taylor, D. L., and Lanni, F. (1993). Enhancement of axial resolution in fluorescence microscopy by standing-wave excitation. *Nature* **366**(6450), 44–48.

Barger, S. W., Horster, D., Furukawa, K., Goodman, Y., Krieglstein, J., and Mattson, M. P. (1995). Tumor-necrosis-factor-alpha and tumor-necrosis-factor-beta protect neurons against amyloid beta-peptide toxicity—evidence for involvement of a kappa-B-binding factor and attenuation of peroxide and Ca2+ accumulation. *Proc. Natl. Acad. Sci. USA* **92**(20), 9328–9332.

Bastiaens, P. I., and Squire, A. (1999). Fluorescence lifetime imaging microscopy: Spatial resolution of biochemical processes in the cell. *Trends Cell Biol.* **9**(2), 48–52.

Becker, W., Bergmann, A., Hink, M. A., Konig, K., Benndorf, K., and Biskup, C. (2004). Fluorescence lifetime imaging by time-correlated single-photon counting. *Microsc. Res. Tech.* **63**(1), 58–66.

Bekker-Jensen, S., Lukas, C., Melander, F., Bartek, J., and Lukas, J. (2005). Dynamic assembly and sustained retention of 53BP1 at the sites of DNA damage are controlled by Mdc1/NFBD1. *J. Cell Biol.* **170**(2), 201–211.

Belaya, K., Tollervey, D., and Kos, M. (2006). FLIPing heterokaryons to analyze nucleo-cytoplasmic shuttling of yeast proteins. *RNA* **12**(5), 921–930.

Berland, K., and Shen, G. (2003). Excitation saturation in two-photon fluorescence correlation spectroscopy. *Appl. Opt.* **42**(27), 5566–5576.

Berland, K. M., So, P. T., and Gratton, E. (1995). Two-photon fluorescence correlation spectroscopy: Method and application to the intracellular environment. *Biophys. J.* **68**(2), 694–701.

Bewersdorf, J., Pick, R., and Hell, S. W. (1998). Multifocal multiphoton microscopy. *Opt. Lett.* **23**(9), 655–657.

Booth, M. J., and Hell, S. W. (1998). Continuous wave excitation two-photon fluorescence microscopy exemplified with the 647-nm ArKr laser line. *J. Microsc.* **190,** 298–304.

Braeckmans, K., Peeters, L., Sanders, N. N., De Smedt, S. C., and Demeester, J. (2003). Three-dimensional fluorescence recovery after photobleaching with the confocal scanning laser microscope. *Biophys. J.* **85**(4), 2240–2252.

Braunagel, S. C., Williamson, S. T., Saksena, S., Zhong, Z., Russell, W. K., Russell, D. H., and Summers, M. D. (2004). Trafficking of ODV-E66 is mediated via a sorting motif and other viral proteins: Facilitated trafficking to the inner nuclear membrane. *Proc. Natl. Acad. Sci. USA* **101,** 8372–8377.

Breusegem, S. Y., Levi, M., and Barry, N. P. (2006). Fluorescence correlation spectroscopy and fluorescence lifetime imaging microscopy. *Nephron Exp. Nephrol.* **103**(2), e41–e49.

Buchler, M., Konig, J., Brom, R., Kartenbeck, J., Spring, H., Horie, T., and Keppler, D. (1996). cDNA cloning of the hepatocyte canalicular isoform of the multidrug resistance protein, cMrp, reveals a novel conjugate export pump deficient in hyperbilirubinemic mutant rats. *J. Biol. Chem.* **271**(25), 15091–15098.

Bulinski, J. C., Odde, D. J., Howell, B. J., Salmon, T. D., and Waterman-Storer, C. M. (2001). Rapid dynamics of the microtubule binding of ensconsin *in vivo*. *J. Cell. Sci.* **114**(Pt. 21), 3885–3897.

Campagnola, P. J., and Loew, L. M. (2003). Second-harmonic imaging microscopy for visualizing biomolecular arrays in cells, tissues and organisms. *Nature Biotech.* **21**(11), 1356–1360.

Campagnola, P. J., Millard, A. C., Terasaki, M., Hoppe, P. E., Malone, C. J., and Mohler, W. A. (2002). Three-dimensional high-resolution second-harmonic generation imaging of endogenous structural proteins in biological tissues. *Biophys. J.* **82,** 493–508.

Carlsson, K., and Aslund, N. (1987). Confocal imaging for 3-D digital microscopy. *Appl. Opt.* **26**(16), 3232–3238.

Carlsson, K., Danielsson, P. E., Lenz, R., Liljeborg, A., Majlof, L., and Aslund, N. (1985). Three-dimensional microscopy using a confocal laser scanning microscope. *Opt. Lett.* **10**(2), 53–55.

Caudron, M., Bunt, G., Bastiaens, P., and Karsenti, E. (2005). Spatial coordination of spindle assembly by chromosome-mediated signaling gradients. *Science* **309**(5739), 1373–1376.

Chen, D., and Huang, S. (2001). Nucleolar components involved in ribosome biogenesis cycle between the nucleolus and nucleoplasm in interphase cells. *J. Cell Biol.* **153**(1), 169–176.

Chen, J. X., Volkmer, A., Book, L. D., and Xie, X. S. (2002). Multiplex coherent anti-stokes Raman scattering microspectroscopy and study of lipid vesicles. *J. Phys. Chem. B* **106**(34), 8493–8498.

Chen, Y., Muller, J. D., Ruan, Q., and Gratton, E. (2002). Molecular brightness characterization of EGFP *in vivo* by fluorescence fluctuation spectroscopy. *Biophys. J.* **82**(1, Pt. 1), 133–144.

Chen, Y., Muller, J. D., So, P. T., and Gratton, E. (1999). The photon counting histogram in fluorescence fluctuation spectroscopy. *Biophys. J.* **77**(1), 553–567.

Chen, Y., and Periasamy, A. (2004). Characterization of two-photon excitation fluorescence lifetime imaging microscopy for protein localization. *Microsc. Res. Tech.* **63**(1), 72–80.

Chen, Y., Tekmen, M., Hillesheim, L., Skinner, J., Wu, B., and Muller, J. D. (2005). Dual-color photon-counting histogram. *Biophys. J.* **88**(3), 2177–2192.

Cheng, H., Lederer, W. J., and Cannell, M. B. (1993). Calcium sparks—elementary events underlying excitation-contraction coupling in heart-muscle. *Science* **262**(5134), 740–744.

Cheng, J. X., and Xie, X. S. (2004). Coherent anti-Stokes Raman scattering microscopy: Instrumentation, theory, and applications. *J. Phys. Chem. B* **108,** 827–840.

Clayton, A. H., Hanley, Q. S., Arndt-Jovin, D. J., Subramaniam, V., and Jovin, T. M. (2002). Dynamic fluorescence anisotropy imaging microscopy in the frequency domain (rFLIM). *Biophys. J.* **83**(3), 1631–1649.

Conchello, J.-A., and Lichtman, J. W. (2005). Optical sectioning microscopy. *Nat. Methods* **2**(12), 920–931.

Condeelis, J., and Segall, J. E. (2003). Intravital imaging of cell movement in tumours. *Nature Rev. Cancer* **3**(12), 921–930.

Curley, P. F., Ferguson, A. I., White, J. G., and Amos, W. B. (1992). Application of a femtosecond self-sustaining mode-locked Ti:sapphire laser to the field of laser scanning confocal microscopy. *Opt. Quantum Electron.* **24**(8), 851–859.

Daigle, N., Beaudouin, J., Hartnell, L., Imreh, G., Hallberg, E., Lippincott-Schwartz, J., and Ellenberg, J. (2001). Nuclear pore complexes form immobile networks and have a very low turnover in live mammalian cells. *J. Cell Biol.* **154**(1), 71–84.

Delbarre, E., Tramier, M., Coppey-Moisan, M., Gaillard, C., Courvalin, J. C., and Buendia, B. (2006). The truncated prelamin A in Hutchinson-Gilford progeria syndrome alters segregation of A-type and B-type lamin homopolymers. *Hum. Mol. Genet.* **15**(7), 1113–1122.

Delon, A., Usson, Y., Derouard, J., Biben, T., and Souchier, C. (2006). Continuous photobleaching in vesicles and living cells: A measure of diffusion and compartmentation. *Biophys. J.* **90**(7), 2548–2562.

Denk, W., and Detwiler, P. B. (1999). Optical recording of light-evoked calcium signals in the functionally intact retina. *Proc. Natl. Acad. Sci. USA* **96,** 7035–7040.

Denk, W., Strickler, J. H., and Webb, W. W. (1990). Two-photon laser scanning fluorescence microscopy. *Science* **248,** 73–76.

Digman, M. A., Brown, C. M., Sengupta, P., Wiseman, P. W., Horwitz, A. R., and Gratton, E. (2005). Measuring fast dynamics in solutions and cells with a laser scanning microscope. *Biophys. J.* **89**(2), 1317–1327.

Dix, J. A., and Verkman, A. S. (1990). Mapping of fluorescence anisotropy in living cells by ratio imaging. Application to cytoplasmic viscosity. *Biophys. J.* **57**(2), 231–240.

Duncan, M. D., Reintjes, J., and Manuccia, T. J. (1982). Scanning coherent anti-Stokes Raman microscope. *Opt. Lett.* **7,** 350–352.

Egner, A., Andresen, V., and Hell, S. (2002). Comparison of the axial resolution of practical Nipkow-disk confocal fluorescence microscopy with that of multifocal multiphoton microscopy: Theory and experiment. *J. Microsc.* **206**(1), 24–32.

Evans, C. L., Potma, E. O., Puoris'haag, M., Cote, D., Lin, C. P., and Xie, X. S. (2005). Chemical imaging of tissue *in vivo* with video-rate coherent anti-Stokes Raman scattering microscopy. *Proc. Natl. Acad. Sci. USA* **102**(46), 16807–16812.

Fainman, Y., Botvinick, E. L., Price, J. H., and Gough, D. A. (2001). 3D quantitative imaging of the microvasculature with the Texas Instruments digital micromirror device. *In* "Spatial Light Modulators: Technology and Applications." San Deigo, CA.

French, T., So, P. T., Dong, C. Y., Berland, K. M., and Gratton, E. (1998). Fluorescence lifetime imaging techniques for microscopy. *Methods Cell Biol.* **56,** 277–304.

Freund, I., and Deutsch, M. (1986). Second-harmonic microscopy of biological tissue. *Opt. Lett.* **11**(2), 94–96.

Freund, I., Deutsch, M., and Sprecher, A. (1986). Connective tissue polarity. Optical second-harmonic microscopy, crossed-beam summation, and small-angle scattering in rat-tail tendon. *Biophys. J.* **50,** 693–712.

Fujita, K., Nakamura, O., Kaneko, T., Kawata, S., Oyamada, M., and Takamatsu, T. (1999). Real-time imaging of two-photon-induced fluorescence with a microlens-array scanner and a regenerative amplifier. *J. Microsc.* **194**(2/3), 528–531.

Gerlich, D., Koch, B., Dupeux, F., Peters, J. M., and Ellenberg, J. (2006). Live-cell imaging reveals a stable cohesin-chromatin interaction after but not before DNA replication. *Curr. Biol.* **16**(15), 1571–1578.

Gingell, D., Heavens, O. S., and Mellor, J. S. (1987). General electromagnetic theory of total internal reflection fluorescence: The quantitative basis for mapping cell-substratum topography. *J. Cell Sci.* **87** (Pt. 5), 677–693.

Goodman, Y. D., Bruce, A. J., Cheng, B., and Mattson, M. P. (1996). Estrogens attenuate and corticosterone exacerbates excitotoxicity, oxidative injury, and amyloid beta-peptide toxicity in hippocampal neurons. *J. Neurochem.* **66**(5), 1836–1844.

Göppert-Meyer, M. (1931). Über Elementarakte mit zwei Quantensprüngen. Göttinger Dissertation. *Ann. Phys.* **9,** 273–294.

Gräf, R., Rietdorf, J., and Zimmermann, T. (2005). "Live Cell Spinning Disk Microscopy." Springer Berlin, Heidelburg.

Grego, S., Cantillana, V., and Salmon, E. D. (2001). Microtubule treadmilling *in vitro* investigated by fluorescence speckle and confocal microscopy. *Biophys. J.* **81**(1), 66–78.

Guo, Y., Savage, H. E., Liu, F., Schantz, S. P., Ho, P. P., and Alfano, R. R. (1999). Subsurface tumor progression investigated by noninvasive optical second harmonic tomography. *Proc. Natl. Acad. Sci. USA* **96,** 10854–10856.

Habuchi, S., Ando, R., Dedecker, P., Verheijen, W., Mizuno, H., Miyawaki, A., and Hofkens, J. (2005). Reversible single-molecule photoswitching in the GFP-like fluorescent protein Dronpa. *Proc. Natl. Acad. Sci. USA* **102**(27), 9511–9516.

Hakansson, M. L., Brown, H., Ghilardi, N., Skoda, R. C., and Meister, B. (1998). Leptin receptor immunoreactivity in chemically defined target neurons of the hypothalamus. *J. Neurosci.* **18**(1), 559–572.

Harpur, A. G., Wouters, F. S., and Bastiaens, P. I. (2001). Imaging FRET between spectrally similar GFP molecules in single cells. *Nat. Biotechnol.* **19**(2), 167–169.

Helmchen, F., and Denk, W. (2005). Deep tissue two-photon microscopy. *Nat. Methods* **2**(12), 932–940.

Hell, S., and Stelzer, E. H. K. (1992a). Fundamental improvement of resolution with a 4Pi-confocal fluorescence microscope using two-photon excitation. *Opt. Commun.* **93,** 277–282.

Hell, S., and Stelzer, E. H. K. (1992b). Properties of a 4Pi confocal fluorescence microscope. *J. Opt. Soc. Am. A* (*Opt. Image Sci.*) **9**(12), 2159–2166.

Hess, S. T., and Webb, W. W. (2002). Focal volume optics and experimental artifacts in confocal fluorescence correlation spectroscopy. *Biophys. J.* **83**(4), 2300–2317.

Howell, B. J., Hoffman, D. B., Fang, G., Murray, A. W., and Salmon, E. D. (2000). Visualization of Mad2 dynamics at kinetochores, along spindle fibers, and at spindle poles in living cells. *J. Cell Biol.* **150**(6), 1233–1250.

Inoué, S. (1995). Foundations of confocal scanned imaging in light microscopy. *In* "Handbook of Biological Confocal Microscopy" (J. Pawley, ed.), pp. 1–17. Plenum Press, New York.

Jacobson, K., Derzko, Z., Wu, E. S., Hou, Y., and Poste, G. (1976). Measurement of the lateral mobility of cell surface components in single, living cells by fluorescence recovery after photobleaching. *J. Supramol. Struct.* **5**(4), 565(417)-576(428).

Jares-Erijman, E. A., and Jovin, T. M. (2003). FRET imaging. *Nat. Biotechnol.* **21**(11), 1387–1395.

Job, C., and Eberwine, J. (2001). Identification of sites for exponential translation in living dendrites. *Proc. Natl. Acad. Sci. USA* **98**(23), 13037–13042.

Kaiser, W., and Garrett, C. G. B. (1961). Two-photon excitation in CaF_2: Eu^{2+}. *Phys. Rev. Lett.* **7**(6), 229.

Kalab, P., Pralle, A., Isacoff, E. Y., Heald, R., and Weis, K. (2006). Analysis of a RanGTP-regulated gradient in mitotic somatic cells. *Nature* **440**(7084), 697–701.

Khodjakov, A., and Rieder, C. L. (1999). The sudden recruitment of gamma-tubulin to the centrosome at the onset of mitosis and its dynamic exchange throughout the cell cycle, do not require microtubules. *J. Cell Biol.* **146**(3), 585–596.

Kim, S. A., Heinze, K. G., Bacia, K., Waxham, M. N., and Schwille, P. (2005). Two-photon cross-correlation analysis of intracellular reactions with variable stoichiometry. *Biophys. J.* **88**(6), 4319–4336.

Kirsch, A. K., Subramaniam, V., Striker, G., Schnetter, C., Arndt-Jovin, D. J., and Jovin, T. M. (1998). Continuous wave two-photon scanning near-field optical microscopy. *Biophys. J.* **75,** 1513–1521.

Kisurina-Evgenieva, O., Mack, G., Du, Q., Macara, I., Khodjakov, A., and Compton, D. A. (2004). Multiple mechanisms regulate NuMA dynamics at spindle poles. *J. Cell Sci.* **117**(Pt. 26), 6391–6400.

Kogure, T., Karasawa, S., Araki, T., Saito, K., Kinjo, M., and Miyawaki, A. (2006). A fluorescent variant of a protein from the stony coral Montipora facilitates dual-color single-laser fluorescence cross-correlation spectroscopy. *Nat. Biotechnol.* **24**(5), 577–581.

Kohler, R. H., Schwille, P., Webb, W. W., and Hanson, M. R. (2000). Active protein transport through plastid tubules: Velocity quantified by fluorescence correlation spectroscopy. *J. Cell Sci.* **113**(Pt. 22), 3921–3930.

Konig, K., Liang, H., Berns, M. W., and Tromberg, B. J. (1995). Cell damage by near-IR microbeams. *Nature* **377**(6544), 20–21.

Krylyshkina, O., Anderson, K. I., Kaverina, I., Upmann, I., Manstein, D. J., Small, J. V., and Toomre, D. K. (2003). Nanometer targeting of microtubules to focal adhesions. *J. Cell Biol.* **161**(5), 853–859.

Lakowicz, J. R. (1999). "Principles of Fluorescence Spectroscopy." Plenum Press, New York.

Larson, D. R., Gosse, J. A., Holowka, D. A., Baird, B. A., and Webb, W. W. (2005). Temporally resolved interactions between antigen-stimulated IgE receptors and Lyn kinase on living cells. *J. Cell Biol.* **171**(3), 527–536.

Larson, D. R., Ma, Y. M., Vogt, V. M., and Webb, W. W. (2003). Direct measurement of Gag-Gag interaction during retrovirus assembly with FRET and fluorescence correlation spectroscopy. *J. Cell Biol.* **162**(7), 1233–1244.

Lawson, N. D., and Weinstein, B. M. (2002). *In vivo* imaging of embryonic vascular development using transgenic zebrafish. *Develop. Biol.* **248**(2), 307–318.

Lele, T. P., and Ingber, D. E. (2006). A mathematical model to determine molecular kinetic rate constants under non-steady state conditions using fluorescence recovery after photobleaching (FRAP). *Biophys. Chem.* **120**(1), 32–35.

Liang, H., Vu, K. T., Krishnan, P., Trang, T. C., Shin, D., Kimel, S., and Berns, M. W. (1996). Wavelength dependence of cell cloning efficiency after optical trapping. *Biophys. J.* **70**(3), 1529–1533.

Lin, Y. Z., Yao, S. Y., Veach, R. A., Torgerson, T. R., and Hawiger, J. (1995). Inhibition of nuclear translocation of transcription factor Nf-kappa-B by a synthetic peptide-containing a cell membrane-permeable motif and nuclear-localization sequence. *J. Biol. Chem.* **270**(24), 14255–14258.

Loerke, D., Preitz, B., Stuhmer, W., and Oheim, M. (2000). Super-resolution measurements with evanescent-wave fluorescence excitation using variable beam incidence. *J. Biomed Opt.* **5**(1), 23–30.

Luby-Phelps, K., and Taylor, D. L. (1988). Subcellular compartmentalization by local differentiation of cytoplasmic structure. *Cell Motil. Cytoskeleton* **10**(1–2), 28–37.

Magde, D., Elson, E., and Webb, W. W. (1972). Thermodynamic fluctuations in a reacting system—measurement by fluorescence correlation spectroscopy. *Phys. Rev. Lett.* **29**(11), 705.

Maria, N., Provitera, V., Crisci, C., Stancancelli, A., Wendelschafer-Crabb, G., Kennedy, W. R., and Santoro, L. (2003). Quantification of myelinated endings and mechanoreceptors in human digital skin. *Ann. Neurol.* **54,** 197–205.

Marrelli, S. P., Eckmann, M. S., and Hunte, M. S. (2003). Role of endothelial intermediate conductance KCa channels in cerebral EDHF-mediated dilations. *Am. J. Physiol. Heart Circ. Physiol.* **285,** H1590–H1599.

Mathur, A. B., Chan, B. P., Truskey, G. A., and Reichert, W. M. (2003). High-affinity augmentation of endothelial cell attachment: Long-term effects on focal contact and actin filament formation. *J. Biomed. Mater. Res. Part A* **66A**(4), 729–737.

Medina, M. A., and Schwille, P. (2002). Fluorescence correlation spectroscopy for the detection and study of single molecules in biology. *Bioessays* **24**(8), 758–764.

Misteli, T., Gunjan, A., Hock, R., Bustin, M., and Brown, D. T. (2000). Dynamic binding of histone H1 to chromatin in living cells. *Nature* **408**(6814), 877–881.

Mitchison, T. J. (1989). Polewards microtubule flux in the mitotic spindle: Evidence from photoactivation of fluorescence. *J. Cell Biol.* **109**(2), 637–652.

Mohler, W. A., Simske, J. S., Williams-Masson, E. M., Hardin, J. D., and White, J. G. (1998). Dynamics and ultrastructure of developmental cell fusions in the *Caenorhabditis elegans* hypodermis. *Curr. Biol.* **8**(19), 1087–1090.

Muller, J. D. (2004). Cumulant analysis in fluorescence fluctuation spectroscopy. *Biophys. J.* **86**(6), 3981–3992.

Muller, M., and Schins, J. M. (2002). Imaging the thermodynamic state of lipid membranes with multiplex CARS microscopy. *J. Phys. Chem. B* **106**(14), 3715–3723.

Nagy, A., Wu, J., and Berland, K. M. (2005). Characterizing observation volumes and the role of excitation saturation in one-photon fluorescence fluctuation spectroscopy. *J. Biomed. Opt.* **10**(4), 44015.

Nakano, A. (2002). Spinning-disk confocal microscopy—a cutting-edge tool for imaging of membrane traffic. *Cell Struct. Funct.* **27**(5), 349–355.

Nan, X. L., Cheng, J. X., and Xie, X. S. (2003). Vibrational imaging of lipid droplets in live fibroblast cells with coherent anti-Stokes Raman scattering microscopy. *J. Lipid Res.* **44**(11), 2202–2208.

Nehls, S., Snapp, E. L., Cole, N. B., Zaal, K. J., Kenworthy, A. K., Roberts, T. H., Ellenberg, J., Presley, J. F., Siggia, E., and Lippincott-Schwartz, J. (2000). Dynamics and retention of misfolded proteins in native ER membranes. *Nat. Cell Biol.* **2**(5), 288–295.

Nielsen, T., Fricke, M., Hellweg, D., and Andresen, P. (2001). High efficiency beam splitter for multifocal multiphoton microscopy. *J. Microsc.* **201**(3), 368–376.

Nitatori, T., Sato, N., Waguri, S., Karasawa, Y., Araki, H., Shibanai, K., Kominami, E., and Uchiyama, Y. (1995). Delayed neuronal death in the Ca1 pyramidal cell layer of the Gerbil Hippocampus following transient ischemia is apoptosis. *J. Neurosci.* **15**(2), 1001–1011.

Oheim, M., Loerke, D., Stuhmer, W., and Chow, R. H. (1998). The last few milliseconds in the life of a secretory granule—docking, dynamics and fusion visualized by total internal reflection fluorescence microscopy (TIRFM). *Eur. Biophys. J. Biophys. Lett.* **27**(2), 83–98.

Ovechkina, Y., Maddox, P., Oakley, C. E., Xiang, X., Osmani, S. A., Salmon, E. D., and Oakley, B. R. (2003). Spindle formation in Aspergillus is coupled to tubulin movement into the nucleus. *Mol. Biol. Cell.* **14**(5), 2192–2200.

Patterson, G. H., and Lippincott-Schwartz, J. (2002). A photoactivatable GFP for selective photolabeling of proteins and cells. *Science* **297**(5588), 1873–1877.

Pearson, C. G., Maddox, P. S., Zarzar, T. R., Salmon, E. D., and Bloom, K. (2003). Yeast kinetochores do not stabilize Stu2p-dependent spindle microtubule dynamics. *Mol. Biol. Cell.* **14**(10), 4181–4195.

Peleg, G., Lewis, A., Linial, M., and Loew, L. M. (1999). Nonlinear optical measurement of membrane potential around single molecules at selected cellular sites. *Proc. Natl. Acad. Sci. USA* **96,** 6700–6704.

Pelet, S., Previte, M. J., and So, P. T. (2006). Comparing the quantification of Forster resonance energy transfer measurement accuracies based on intensity, spectral, and lifetime imaging. *J. Biomed. Opt.* **11**(3), 34017-1–34017-11.

Peter, M., Ameer-Beg, S. M., Hughes, M. K., Keppler, M. D., Prag, S., Marsh, M., Vojnovic, B., and Ng, T. (2005). Multiphoton-FLIM quantification of the EGFP-mRFP1 FRET pair for localization of membrane receptor-kinase interactions. *Biophys. J.* **88**(2), 1224–1237.

Petrán, M., Hadravský, M., Egger, M. D., and Galambos, R. (1968). Tandem-scanning reflected-light microscope. *J. Opt. Soc. Am.* **58,** 661–664.

Potma, E. O., De Boeij, W. P., Van Haastert, P. J. M., and Wiersma, D. A. (2001). Real-time visualization of intracellular hydrodynamics in single living cells. *Proc. Natl. Acad. Sci. USA* **98**(4), 1577–1582.

Ramdya, P., Skoch, J., Bacskai, B. J., Hyman, B. T., and Berezovska, O. (2003). Activated Notch1 associates with a presenilin-1/gamma-secretase docking site. *J. Neurochem.* **87**(4), 843–850.

Reichert, W. M., and Truskey, G. A. (1990). Total internal reflection fluorescence (TIRF) microscopy. I. Modelling cell contact region fluorescence. *J. Cell Sci.* **96,** 219–230.

Ries, J., and Schwille, P. (2006). Studying slow membrane dynamics with continuous wave scanning fluorescence correlation spectroscopy. *Biophys. J.* **91**(5), 1915–1924.

Rohrbach, A. (2000). Observing secretory granules with a multiangle evanescent wave microscope. *Biophys. J.* **78**(5), 2641–2654.

Salic, A., Waters, J. C., and Mitchison, T. J. (2004). Vertebrate shugoshin links sister centromere cohesion and kinetochore microtubule stability in mitosis. *Cell* **118**(5), 567–578.

Salmon, W. C., Adams, M. C., and Waterman-Storer, C. M. (2002). Dual-wavelength fluorescent speckle microscopy reveals coupling of microtubule and actin movements in migrating cells. *J. Cell Biol.* **158,** 31–37.

Schwille, P., Haupts, U., Maiti, S., and Webb, W. W. (1999). Molecular dynamics in living cells observed by fluorescence correlation spectroscopy with one- and two-photon excitation. *Biophys. J.* **77**(4), 2251–2265.

Shah, J. V., Botvinick, E., Bonday, Z., Furnari, F., Berns, M., and Cleveland, D. W. (2004). Dynamics of centromere and kinetochore proteins; implications for checkpoint signaling and silencing. *Curr. Biol.* **14**(11), 942–952.

Shaner, N. C., Steinbach, P. A., and Tsien, R. Y. (2005). A guide to choosing fluorescent proteins. *Nat. Methods* **2**(12), 905–909.

Sheppard, C. J. R., and Kompfner, R. (1978). Resonant scanning optical microscope. *Appl. Opt.* **17**(18), 2879–2882.

Shimi, T., Koujin, T., Segura-Totten, M., Wilson, K. L., Haraguchi, T., and Hiraoka, Y. (2004). Dynamic interaction between BAF and emerin revealed by FRAP, FLIP, and FRET analyses in living HeLa cells. *J. Struct. Biol.* **147**(1), 31–41.

Shimozono, S., Hosoi, H., Mizuno, H., Fukano, T., Tahara, T., and Miyawaki, A. (2006). Concatenation of cyan and yellow fluorescent proteins for efficient resonance energy transfer. *Biochemistry* **45**(20), 6267–6271.

Sisan, D. R., Arevalo, R., Graves, C., Mcallister, R., and Urbach, J. S. (2006). Spatially-resolved fluorescence correlation spectroscopy using a spinning disk confocal microscope. *Biophys. J.* **106,** 4241–4252.

Skinner, J. P., Chen, Y., and Muller, J. D. (2005). Position-sensitive scanning fluorescence correlation spectroscopy. *Biophys. J.* **89**(2), 1288–1301.

Smith, P. J., Taylov, C. M., Shaw, A. J., and Mccabe, E. M. (2000). Programmable array microscopy with a ferroelectric liquid-crystal spatial light modulator. *Appl. Opt.* **39**(16), 2664–2669.

Spector, D. L., Fu, X. D., and Maniatis, T. (1991). Associations between distinct pre-messenger-RNA splicing components and the cell-nucleus. *EMBO J.* **10**(11), 3467–3481.

Sprague, B. L., Pego, R. L., Stavreva, D. A., and Mcnally, J. G. (2004). Analysis of binding reactions by fluorescence recovery after photobleaching. *Biophys. J.* **86**(6), 3473–3495.

Stout, A. L., and Axelrod, D. (1989). Evanescent field excitation of fluorescence by epi-illumination microscopy. *Appl. Opt.* **28**(24), 5237–5242.

Straub, M., and Hell, S. W. (1998). Multifocal multiphoton microscopy: A fast and efficient tool for 3-D fluorescence imaging. *Bioimaging* **6**(4), 177–184.

Svelto, O. (1998). ''Principles of Lasers.'' Plenum Press, New York.

Svoboda, K., Denk, W., Kleinfeld, D., and Tank, D. W. (1997). *In vivo* dendritic calcium dynamics in neocortical pyramidal neurons. *Nature* **385**(6612), 161–165.

Tanaami, T., Otsuki, S., Tomosada, N., Kosugi, Y., Shimizu, M., and Ishida, H. (2002). High-speed 1-frame/ms scanning confocal microscope with a microlens and Nipkow disks. *Appl. Opt.* **41**(22), 4704–4708.

Theriot, J. A., and Mitchison, T. J. (1991). Actin microfilament dynamics in locomoting cells. *Nature* **352**(6331), 126–131.

Thews, E., Gerken, M., Eckert, R., Zapfel, J., Tietz, C., and Wrachtrup, J. (2005). Cross talk free fluorescence cross correlation spectroscopy in live cells. *Biophys. J.* **89**(3), 2069–2076.

Tirnauer, J. S., Canman, J. C., Salmon, E. D., and Mitchison, T. J. (2002). EB1 targets to kinetochores with attached, polymerizing microtubules. *Mol. Biol. Cell* **13,** 4308–4316.

Tolles, W. M., Nibler, J. W., Mcdonald, J. R., and Harvey, A. B. (1977). Review of theory and application of coherent anti-Stokes Raman-spectroscopy (Cars). *Appl. Spectrosc.* **31**(4), 253–271.

Tsien, R., and Waggoner, A. (1995). Fluorophores for confocal microscopy: Photophysics and photochemistry. *In* ''Handbook of Biological Confocal Microscopy'' (J. Pawley, ed.), pp. 267–279. Plenum Press, New York.

Tsien, R. Y. (1998). The green fluorescent protein. *Annu. Rev. Biochem.* **67,** 509–544.

Tsutsui, H., Karasawa, S., Shimizu, H., Nukina, N., and Miyawaki, A. (2005). Semi-rational engineering of a coral fluorescent protein into an efficient highlighter. *EMBO Rep.* **6**(3), 233–238.

Verveer, P. J., Hanley, Q. S., Verbeek, P. W., Van Vliet, L. J., and Jovin, T. M. (1998). Theory of confocal fluorescence imaging in the programmable array microscope (PAM). *J. Microsc.* **189,** 192–198.

Volkmer, A., Subramaniam, V., Birch, D. J., and Jovin, T. M. (2000). One- and two-photon excited fluorescence lifetimes and anisotropy decays of green fluorescent proteins. *Biophys. J.* **78**(3), 1589–1598.

Von Wichert, G., Haimovich, B., Feng, G. S., and Sheetz, M. P. (2003). Force-dependent integrin-cytoskeleton linkage formation requires downregulation of focal complex dynamics by Shp2. *EMBO J.* **22**(19), 5023–5035.

Wachsmuth, M., Weidemann, T., Muller, G., Hoffmann-Rohrer, U. W., Knoch, T. A., Waldeck, W., and Langowski, J. (2003). Analyzing intracellular binding and diffusion with continuous fluorescence photobleaching. *Biophys. J.* **84**(5), 3353–3363.

Wadsworth, P. (1999). Regional regulation of microtubule dynamics in polarized, motile cells. *Cell Motil. Cytoskeleton* **42**(1), 48–59.

Wang, H. F., Fu, Y., Zickmund, P., Shi, R. Y., and Cheng, J. X. (2005). Coherent anti-stokes Raman scattering imaging of axonal myelin in live spinal tissues. *Biophys. J.* **89**(1), 581–591.

Wang, W., Wyckoff, J. B., Frohlich, V. C., Oleynikov, Y., Hüttelmaier, S., Zavadil, J., Cermak, L., Bottinger, E. P., Singer, R. H., White, J. G., Segall, J. E., and Condeelis, J. S. (2002). Single cell behavior in metastatic primary mammary tumors correlated with gene expression patterns revealed by molecular profiling. *Cancer Res.* **62**(21), 6278–6288.

Wang, Z., Shah, J. V., Berns, M. W., and Cleveland, D. W. (2006). *In vivo* quantitative studies of dynamic intracellular processes using fluorescence correlation spectroscopy. *Biophys. J.* **91**(1), 343–351.

Wang, Z., Shah, J. V., Chen, Z., Sun, C. H., and Berns, M. W. (2004). Fluorescence correlation spectroscopy investigation of a GFP mutant-enhanced cyan fluorescent protein and its tubulin fusion in living cells with two-photon excitation. *J. Biomed. Opt.* **9**(2), 395–403.

Weiss, M., Hashimoto, H., and Nilsson, T. (2003). Anomalous protein diffusion in living cells as seen by fluorescence correlation spectroscopy. *Biophys. J.* **84**(6), 4043–4052.

White, J. G., Amos, W. B., and Fordham, M. (1987). An evaluation of confocal versus conventional imaging of biological structures by fluorescence light microscopy. *J. Cell Biol.* **105,** 41–48.

Wiedenmann, J., Ivanchenko, S., Oswald, F., Schmitt, F., Rocker, C., Salih, A., Spindler, K.-D., and Nienhaus, G. U. (2004). EosFP, a fluorescent marker protein with UV-inducible green-to-red fluorescence conversion. *PNAS* **101**(45), 15905–15910.

Wilson, T. (1980). Imaging properties and applications of scanning optical microscopes. *Appl. Phys. A: Mater. Sci. Process.* **22**(2), 119–128.

Wilson, T., Gannaway, J. N., and Johnson, P. (1980). A scanning optical microscope for the inspection of semiconductor materials and devices. *J. Microsc.* **118**(3), 309–314.

Wolf, K., Mazo, I., Leung, H., Engelke, K., Von Andrian, U. H., Deryugina, E. I., Strongin, A. Y., Brocker, E. B., and Friedl, P. (2003). Compensation mechanism in tumor cell migration: Mesenchymal-amoeboid transition after blocking of pericellular proteolysis. *J. Cell Biol.* **160**(2), 267–277.

Yaffe, M. P., Stuurman, N., and Vale, R. D. (2003). Mitochondrial positioning in fission yeast is driven by association with dynamic microtubules and mitotic spindle poles. *Proc. Natl. Acad. Sci. USA* **100**(20), 11424–11428.

Yvon, A. M. C., and Wadsworth, P. (2000). Region-specific microtubule transport in motile cells. *J. Cell Biol.* **151**(5), 1003–1012.

Zhang, J., Campbell, R. E., Ting, A. Y., and Tsien, R. Y. (2002). Creating new fluorescent probes for cell biology. *Nat. Rev. Mol. Cell Biol.* **3**(12), 906–918.

Zipfel, W. R., Williams, R. M., and Webb, W. W. (2003). Nonlinear magic: Multiphoton microscopy in the biosciences. *Nat. Biotechnol.* **21**(11), 1369–1377.

Zoumi, A., Yeh, A., and Tromberg, B. J. (2002). Imaging cells and extracellular matrix *in vivo* by using second-harmonic generation and two-photon excited fluorescence. *Proc. Natl. Acad. Sci. USA* **99,** 11014–11019.